THE JOURNAL OF BIOLOGICAL CHEMISTRY VOL. 290, NO. 23, pp. 14289–14301, June 5, 2015

Phosphatidylinositol 4,5-Bisphosphate Homeostasis Regulated by Nir2 and Nir3 Proteins at Endoplasmic Reticulum-Plasma Membrane Junctions*[S]

Received for publication, October 23, 2014, and in revised form, April 8, 2015 Published, JBC Papers in Press, April 17, 2015, DOI 10.1074/jbc.M114.621375

Chi-Lun Chang and Jen Liou[1]

From the Department of Physiology, University of Texas Southwestern Medical Center, Dallas, Texas 75390

Background: Mechanisms coupling phosphatidylinositol (PI) 4,5-bisphosphate (PIP_2) hydrolysis to its rapid replenishment remain elusive.
Results: Phosphatidic acid production triggers PIP_2 replenishment mediated by Nir2 and Nir3 at endoplasmic reticulum (ER)-plasma membrane (PM) junctions with PI at the ER membrane.
Conclusion: Nir2 and Nir3 are feedback regulators for PIP_2 homeostasis.
Significance: Nir2 and Nir3 maintain PIP_2 homeostasis via a nonvesicular mechanism at ER-PM junctions.

Phosphatidylinositol (PI) 4,5-bisphosphate (PIP_2) at the plasma membrane (PM) constitutively controls many cellular functions, and its hydrolysis via receptor stimulation governs cell signaling. The PI transfer protein Nir2 is essential for replenishing PM PIP_2 following receptor-induced hydrolysis, but key mechanistic aspects of this process remain elusive. Here, we demonstrate that PI at the membrane of the endoplasmic reticulum (ER) is required for the rapid replenishment of PM PIP_2 mediated by Nir2. Nir2 detects PIP_2 hydrolysis and translocates to ER-PM junctions via binding to phosphatidic acid. With distinct phosphatidic acid binding abilities and PI transfer protein activities, Nir2 and its homolog Nir3 differentially regulate PIP_2 homeostasis in cells during intense receptor stimulation and in the resting state, respectively. Our study reveals that Nir2 and Nir3 work in tandem to achieve different levels of feedback based on the consumption of PM PIP_2 and function at ER-PM junctions to mediate nonvesicular lipid transport between the ER and the PM.

Phosphatidylinositol (PI)[2] 4,5-bisphosphate (PIP_2) located at the inner leaflet of the plasma membrane (PM) governs many cellular functions, including endocytosis, cytoskeleton dynamics, store-operated Ca^{2+} entry (SOCE), as well as the activities of many small GTPase and ion transporters (1, 2). PIP_2 is generated by sequential phosphorylation of PI originating from the endoplasmic reticulum (ER). PI 4-kinases first phosphorylate PI to generate PI 4-phosphate (PI4P), which is a substrate for PI4P 5-kinases to synthesize PIP_2. PM harbors PI 4-kinase and PI4P 5-kinases to generate PIP_2 from PI and PI4P (1, 3). PI at the ER membrane may be delivered to the PM for PIP_2 synthesis via nonvesicular transport by PI transfer proteins (PITPs) (4). In addition, vesicular transport has been shown to deliver PI4P from the Golgi apparatus to support basal PIP_2 levels at the PM (5).

In response to extracellular stimuli, receptor activation induces hydrolysis of PIP_2 via phospholipase C (PLC) and generates inositol 1,4,5-triphosphate and diacylglycerol (DAG) that trigger downstream Ca^{2+} signaling and protein kinase C activation, respectively (1). DAG can be phosphorylated by DAG kinases (DGKs) to generate another signaling messenger, phosphatidic acid (PA) (6). It has been shown that PM PIP_2 levels rapidly recover within minutes following receptor-induced hydrolysis (7), suggesting that a feedback loop coupling PIP_2 hydrolysis to its replenishment exists to maintain PIP_2-dependent cellular functions. Nevertheless, the molecular mechanisms underlying this feedback remain unclear.

We have previously shown that a PITP Nir2 translocates to ER-PM junctions, where the ER forms close contacts with the PM and promotes PIP_2 replenishment following receptor activation (8). Although Nir2 has been shown to transfer PI between membranes *in vitro* (9), *in vivo* evidence supporting inter-organelle lipid transfer mediated by Nir2 or other PITPs is missing. In this study, we devise approaches to selectively manipulate PIP_2 precursors at the ER and Golgi, and we demonstrate that Nir2-mediated PM PIP_2 replenishment is dependent on PI at the ER membrane. We further demonstrate that Nir2 and its homolog, Nir3, sense PIP_2 hydrolysis and translocate to ER-PM junctions by binding to PA. Finally, we demonstrate differential roles of Nir2 and Nir3 in regulating PIP_2 homeostasis; Nir2 mediates substantial PIP_2 replenishment during intense receptor stimulation to support cell signaling, whereas Nir3 preferentially sustains basal PM PIP_2 levels by sensing subtle PA production in cells in the resting state.

* This work was supported by Welch Foundation Grant I-1789 and by Howard Hughes Medical Institute Graduate Grant 56006776 (to the Mechanisms of Disease and Translational Science Ph.D. Track).
[S] This article contains supplemental Movies 1–4 and Table 1.
[1] Sowell Family Scholar in Medical Research. To whom correspondence should be addressed: Dept. of Physiology, UT Southwestern Medical Center, 6001 Forest Park Rd., Dallas, TX 75390. E-mail: jen.liou@utsouthwestern.edu.
[2] The abbreviations used are: PIP_2, phosphatidylinositol 4,5-bisphosphate; PM, plasma membrane; SOCE, store-operated Ca^{2+} entry; PI, phosphatidylinositol; ER, endoplasmic reticulum; PI4P, PI 4-phosphate; PITP, PI transfer protein; PLC, phospholipase C; DAG, diacylglycerol; DGK, DAG kinase; PA, phosphatidic acid; BFA, brefeldin A; PI-PLC, PI-specific PLC; CFP, cyan fluorescence protein; YFP, yellow fluorescence protein; mCherry, monomeric red fluorescence protein; FKBP, FK506 binding protein; FRB, FKBP-rapamycin binding; H1R, H1 receptor; FM, FFAT mutant; N2-N3, Nir2PITP-Nir3; N3-N2, Nir3PITP-Nir2; PC, phosphatidylcholine.

Together, our findings reveal feedback mechanisms that couple PIP_2 hydrolysis to its replenishment via Nir2 and Nir3 at ER-PM junctions.

Experimental Procedures

Reagents—Thapsigargin, Pluronic F-127, NP-EGTA, and Fura-2 AM were purchased from Invitrogen. All chemicals for extracellular buffer (ECB, 125 mM NaCl, 5 mM KCl, 1.5 mM $MgCl_2$, 20 mM HEPES, 10 mM glucose, and 1.5 mM $CaCl_2$, pH 7.4), penicillin and streptomycin solution, rapamycin, histamine, brefeldin A (BFA), U73122, R59022, and EGTA were obtained from Sigma. Phosphatidic acid (PA, catalog no. 840074) and phosphatidylcholine (PC, catalog no. 252266) were purchased from Avanti Polar Lipids (Alabaster, AL). *o*-[^{32}P]Phosphate was purchased from PerkinElmer Life Sciences. Monoclonal anti-PIP_2 antibody (clone 2C11) was obtained from Echelon Bioscience (Salt Lake City, UT). Human cDNA library and small interfering RNA (siRNA) used in this study were generated as described previously (10). Primers used for siRNA generation are listed in supplemental Table S1.

Cell Culture and Transfection—HeLa cells purchased from ATCC (Manassas, VA) were cultured in minimal essential medium supplemented with 10% FBS (HyClone, Logan, UT) and penicillin and streptomycin solution. DNA plasmids (15–50 ng) and siRNAs (10–25 nM) were transfected into HeLa cells with TransIT-LT1 reagent for 16–20 h and TransIT-TKO reagent for 48–72 h, respectively (Muris, Madison, WI).

DNA Constructs—mCherry-TM-FRB, Nir2-mCherry, MAPPER, Nir2-FM-mCherry, YFP-STIM1, and mCherry-K Ras tail were described previously (8). Nir2-YFP was constructed by replacing the mCherry portion of Nir2-mCherrry with YFP. CFP-FKBP-PI-PLC was cloned by replacing the INP54 part of CFP-FKBP-INP54 with a PCR fragment containing a bacterial PI-PLC from *Listeria monocytogenes* strain 10403S (11, 12). CFP-FKBP-PI-PLC-H86A was generated using QuikChange site-direct mutagenesis kit (Agilent Technologies, Santa Clara, CA). mRFP-FKBP-Sac1-PI-PLC was cloned by replacing the INPP5E part of the Pseudojanin construct with PI-PLC (13). Nir3-mCherry was cloned by replacing the Nir2 part of Nir2-mCherry with PCR fragments retrieved from a human cDNA library containing full-length Nir3 (isoform 2, AB385472). Nir3-YFP was generated by replacing the mCherry portion of Nir3-mCherrry with YFP. Nir2-PITP-mCherry was cloned by replacing the Nir2 part of Nir2-mCherry with a PCR fragment containing amino acid residues 1–263 of Nir2. The C-terminal regions of Nir2 (amino acid residue 911–1244) and Nir3 (amino acid residue 990–1349) were cloned into pSKB2 bacterial expression vector containing His tags at the N terminus. Other mutants of Nir2 and Nir3 were generated using QuikChange site-directed mutagenesis kit. Nir2PITP-Nir3 (N2-N3)-YFP and N2-N3-mCherry were cloned by replacing the Nir2 portion of Nir2-YFP and Nir2-mCherry, respectively, with a Nir2 PCR fragment containing amino acid residues 1–263 and an Nir3 PCR fragment containing amino acid residues 265–1349 using the In-Fusion-HD cloning kit (Clontech). Nir3PITP-Nir2 (N3-N2)-YFP and N3-N2-mCherry were generated using the same backbone plasmids as N2-N3-YFP and N2-N3-mCherry with a Nir3 PCR fragment containing amino acid residues 1–264 and an Nir2 PCR fragment containing amino acid residues 264–1244 by In-Fusion-HD cloning kit. All constructs listed here were verified by sequencing. All oligonucleotides used in this study are listed in supplemental Table S1.

Live Cell Confocal and TIRF Microscopy—HeLa cells were cultured on Lab-Tek chambered no. 1 coverglass (NUNC, Rochester, NY). Before imaging, cells were washed with ECB. Live cell confocal and TIRF imaging experiments were performed at room temperature with 60× or 100× objectives and a confocal TIRF microscope custom-built using a Nikon Eclipse Ti microscope (Melville, NY). The microscope was controlled by Micro-Manager software (14). For inhibitor experiments, HeLa cells were pretreated with 1 μM U73122 or 25 μM R59022 for 1 h or with 5 μg/ml BFA for 10 min. To increase cytosolic Ca^{2+} levels, HeLa cells were loaded with 20 μM NP-EGTA in ECB containing 0.05% Pluronic F-127 and 0.1% of BSA at room temperature for 30 min. Loaded cells were washed with ECB containing 0.1% BSA and incubated in ECB for another 15–30 min before the experiments. To release Ca^{2+} from NP-EGTA, cells were exposed to a 405-nm laser pulse for 400–800 ms at rates of 6 or 10 s per frame.

Protein Translocation to ER-PM Junctions—For the analyses of relative protein translocation to ER-PM junctions, puncta of Nir2, Nir3, or STIM1 from TIRF images were selected. The intensity traces of the selected puncta from the same cell were background-subtracted, normalized to time 0, and averaged. Maximal translocation of Nir2 and Nir3 to ER-PM junctions was determined by measuring the maximal values of the Nir2 and Nir3 translocation traces.

PIP_2 Measurements—Dynamic changes of PIP_2 at the PM during receptor stimulation were determined by the relative intensity of GFP-PLCδ-PH monitored by TIRF microscopy in HeLa cells overexpressing histamine H1 receptor (H1R). An ND8 filter was introduced to the light path to prevent photobleaching. Basal PM PIP_2 levels were determined by the ratio of the intensity of GFP-PLCδ-PH at the PM to that in the cytosol using confocal images of cells with similar adherent surfaces to prevent artifacts caused by the size and the shape of the cells. For direct measurements of PIP_2 using immunostaining, monoclonal anti-PIP_2 antibody (clone 2C11) was used following a previously described protocol (15). Confocal images of the stained cells were taken, and the intensity of PM regions was quantified and normalized to control cells before histamine treatment. For PIP_2 mass analysis, HeLa cells on 6-well plates were labeled *o*-[^{32}P]phosphate (20 μCi/ml) for 4 h in phosphate-free DMEM supplemented with 10% dialyzed FBS. The labeling media were aspirated, and the reaction was terminated by addition of a 500-μl mixture of MeOH and 1 M HCl (1:1 v/v). Cells were then scraped and transferred into tubes, and 250 μl of chloroform was added to extract lipids. The samples were vortexed, centrifuged, and the phospholipids in the lower (organic) phase were obtained by removing the upper phase. The phospholipids were washed with a 250-μl mixture of MeOH and 1 M HCl (1:1). The extracted phospholipids were then separated by thin layer chromatography (TLC) in *n*-propyl alcohol/H_2O/NH_4Cl (65:20:15) solvent system as described

previously (16). TLC plates were exposed to x-ray films. Radioactive PIP_2 levels were quantified by densitometry analysis (ImageJ) and normalized to total ^{32}P-labeled phospholipids.

Liposome Sedimentation Assay—His-tagged C-terminal regions of Nir2 and Nir3 were expressed in BL21(DE3) bacterial cells. Cells were then harvested and lysed in 50 mM Tris buffer, pH 8.0, containing 300 mM NaCl, DNase I, and protease inhibitors. The expressed proteins were purified using Talon cobalt columns (Clontech). The buffer of the purified proteins was exchanged to PIPES buffer (20 mM PIPES, pH 6.8, 137 mM NaCl, 3 mM KCl) using Amicon centrifugal filters (Millipore). Purified proteins were then centrifuged at 22,000 × *g* for 10 min at 4 °C to remove aggregates. To prepare liposomes, PC and PA (in chloroform) were mixed at the ratio as indicated, dried first under nitrogen, then desiccated overnight, and resuspended in buffer containing 20 mM Tris, pH 7.5, and 100 mM NaCl to a final concentration of 1 mg/ml. Liposomes were generated by vortexing and freezing-sonicating the resuspended lipids until clear solutions were formed. Liposomes (20 μl) were mixed with proteins (5 μg in 50 μl in the buffer for liposomes) and incubated for 10 min at room temperature. Proteins bound to the liposomes were sedimented by centrifugation at 16,000 × *g* for 30 min at 4 °C. Proteins in the pellets (liposome-bound) were resuspended in the initial volume of the sample, and equal volumes of the pellets and the supernatants were resolved on SDS-PAGE and detected by GelCode Blue Safe protein stain (Pierce).

Cytosolic Ca^{2+} Level Measurements—HeLa cells were loaded with 0.5 μM Fura-2 AM in ECB containing 0.05% pluronic F-127 and 0.1% of BSA for 30 min at room temperature. Loaded cells were then washed with ECB containing 0.1% BSA and incubated in ECB for another 15–30 min before the experiments. Single-cell Ca^{2+} images were taken with a 4× objective and an automated microscope custom built on a Nikon Eclipse Ti microscope. Changes of intracellular Ca^{2+} levels were indicated by the change of ratio to 510 nm excited at 340 nm to those at 380 nm (F_{340}/F_{380}). For periodic histamine stimulation experiments, Fura-2 loaded cells were placed in a perfusion system built in the laboratory providing a constant ECB flow of 1.5 to 2 ml per min.

Statistical Analyses—Data were statistically analyzed by *t* test or one-way analysis of variance using SigmaPlot software (Systat Software Inc., San Jose, CA).

Results

PI at the ER Membrane Contributes to the Rapid Replenishment of PM PIP_2 Hydrolyzed following Receptor Stimulation—PI originating from the ER is a precursor lipid for PIP_2 synthesis at the PM. To determine whether PI at the ER membrane contributes to the rapid PIP_2 replenishment following receptor-induced hydrolysis, we devised a rapamycin-inducible approach to acutely remove PI at the ER membrane using a bacterial PI-specific PLC (PI-PLC) (Fig. 1*A*). This PI-PLC selectively hydrolyzes PI to generate DAG, and its expression in the cytosol minimally affects cellular PI and PIP_2 levels (12). CFP-FKBP-PI-PLC and CFP-FKBP-PI-PLC-H86A were generated by cloning PI-PLC or its catalytic inactive mutant PI-PLC-H86A into a backbone plasmid containing a cyan fluorescence protein (CFP) and an FK50-binding protein (FKBP) domain at the N terminus. The PI-depleting abilities of these two cytosolic fusion proteins were verified by co-expression with GFP-PKD-C1ab, a high affinity DAG sensor (12), which detected numerous small mobile structures in cells expressing CFP-FKBP-PI-PLC but not in those expressing CFP-FKBP-PI-PLC-H86A

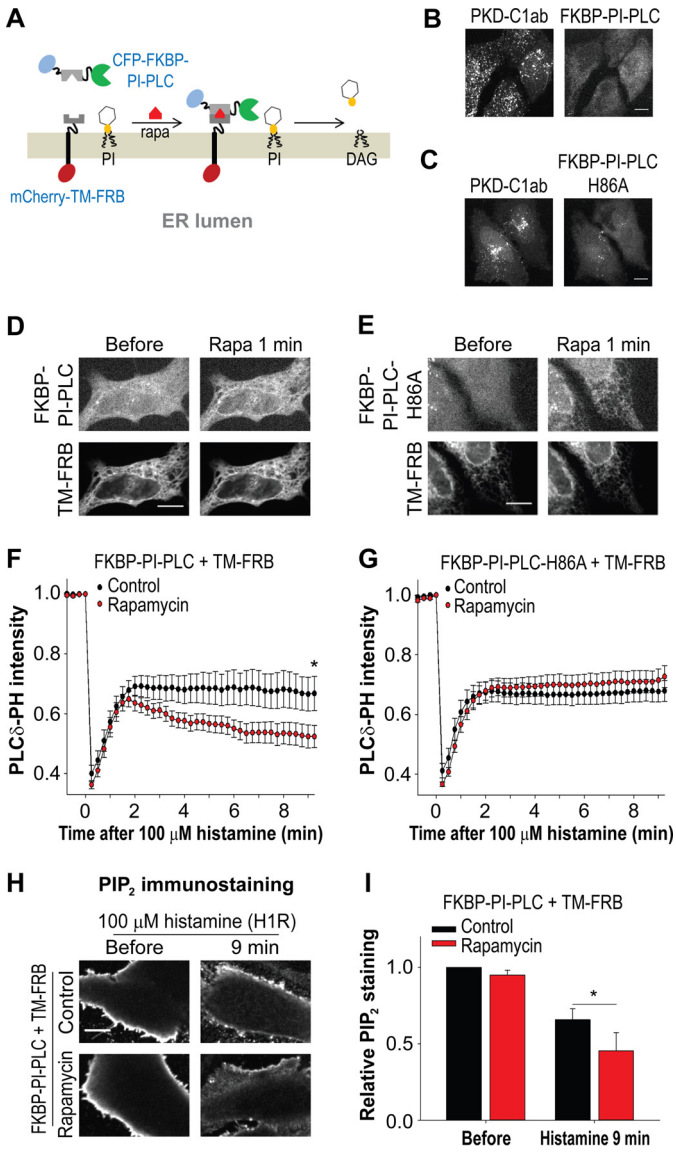

FIGURE 1. **PI at the ER membrane contributes to rapid PM PIP_2 replenishment following receptor-induced hydrolysis.** *A,* diagram of a rapamycin-inducible approach for selective depletion of PI at the ER membrane. *B* and *C,* confocal images of HeLa cells co-expressing GPF-PKD-C1ab and CFP-FKBP-PI-PLC (*B*) or CFP-FKBP-PI-PLC-H86A (*C*). *Scale bar,* 10 μm. *D* and *E,* CFP-FKBP-PI-PLC (*D*) or CFP-FKBP-PI-PLC-H86A (*E*) translocation to the ER induced by 5 μM rapamycin (*Rapa*) monitored by confocal microscopy in a HeLa cell co-expressing mCherry-TM-FRB. *Scale bar,* 10 μm. *F* and *G,* changes in PM PIP_2 levels in HeLa cells co-transfected with H1R, GFP-PLCδ-PH, mCherry-TM-FRB, and CFP-FKBP-PI-PLC (*F*) or CFP-FKBP-PI-PLC-H86A (*G*) in the absence (control) or presence of 5 μM rapamycin pretreatment for 10 min. Means ± S.E. are shown (12–15 cells from three independent experiments). *, $p < 0.05$. *H,* confocal images of PIP_2 immunostaining in HeLa cells expressing H1R, CFP-FKBP-PI-PLC, and mCherry-TM-FRB before or 9 min after histamine stimulation in the absence (control) or presence of rapamycin pretreatment for 10 min. *Scale bar,* 10 μm. *I,* relative PM PIP_2 levels monitored by PIP_2 immunostaining and confocal microscopy as described in *H*. Mean ± S.D. are shown (three independent experiments). *, $p < 0.05$.

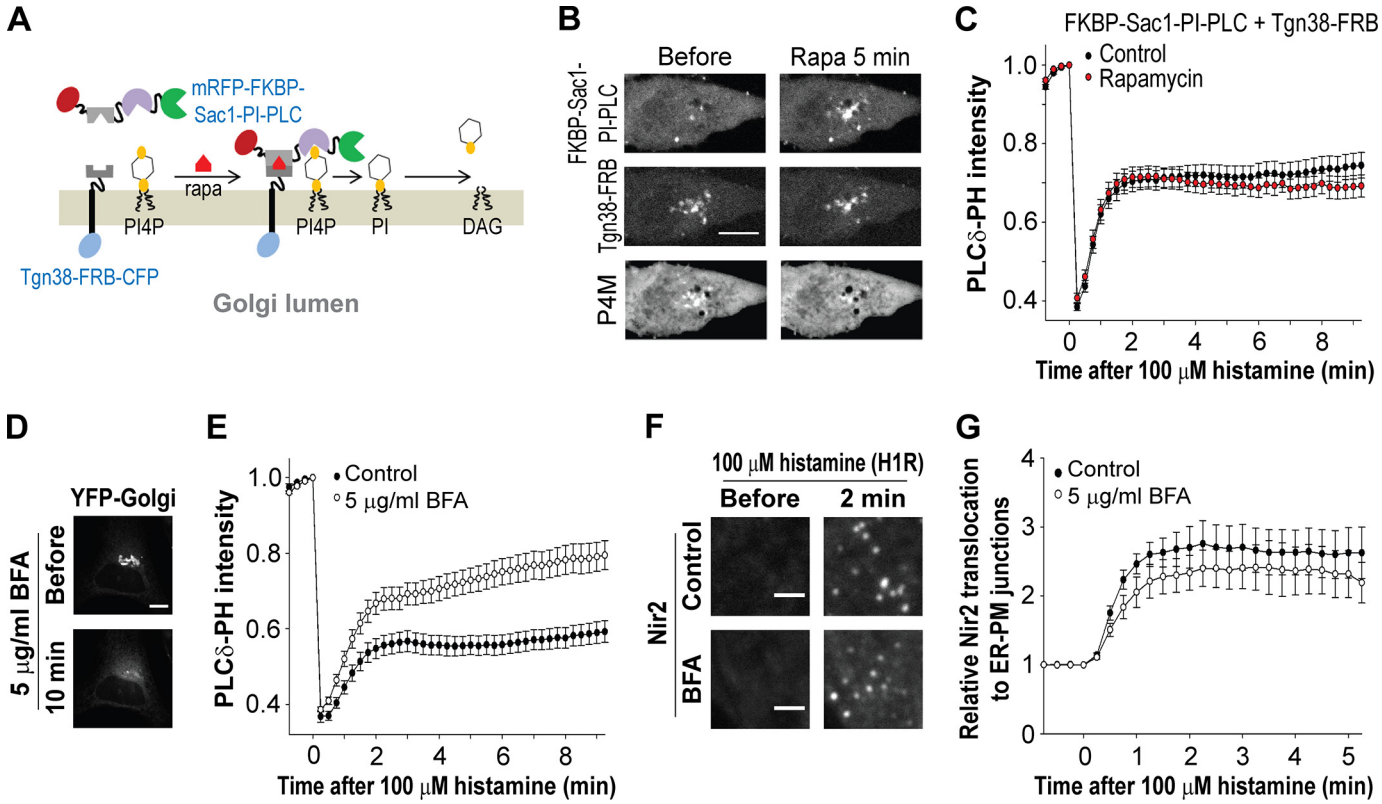

FIGURE 2. **Disruption of PI and PI4P delivery by vesicular transport did not prevent the rapid replenishment of PM PIP$_2$.** *A,* diagram of a rapamycin-inducible approach for selective depletion of PI4P and PI at the Golgi apparatus. *B,* mRFP-FKBP-Sac1-PI-PLC translocation to the Golgi apparatus and PI4P depletion induced by 5 μM rapamycin (*rapa*) monitored by confocal microscopy in a HeLa cell co-expressing Tgn38-FRB-CFP and GFP-P4M. *Scale bar,* 10 μm. *C,* histamine-induced changes in PM PIP$_2$ levels monitored in HeLa cells co-transfected with H1R, GFP-PLCδ-PH, mRFP-FKBP-Sac1-PI-PLC, and Tgn38-FRB-CFP in the absence (control) or presence of 5 μM rapamycin pretreatment for 10 min. Means ± S.E. are shown (19–26 cells from three independent experiments). *D,* disappearance of the Golgi apparatus following 5 μg/ml BFA treatment in a HeLa cell expressing YFP-Golgi monitored by confocal microscopy. *Scale bar,* 10 μm. *E,* dynamic changes of GFP-PLCδ-PH intensity induced by histamine monitored by TIRF microscopy in HeLa cells expressing H1R in the absence (control) or presence of 5 μg/ml BFA pretreatment for 10 min. Means ± S.E. are shown (16–22 cells from three independent experiments). *F,* Nir2-mCherry translocation to ER-PM junctions induced by histamine monitored by TIRF microscopy in HeLa cells transfected with H1R in the absence (control) or presence of 5 μg/ml BFA pretreatment for 10 min. *Scale bar,* 2 μm. *G,* relative translocation of Nir2 to ER-PM junctions monitored by TIRF microscopy in HeLa cells as described in *F.* Means ± S.E. are shown (8–10 cells from two independent experiments).

(Fig. 1, *B* and *C*). Targeting PI-PLC to the cytosolic surface of ER has been shown to efficiently reduce cellular PI levels (12). We applied rapamycin to recruit CFP-FKBP-PI-PLC or CFP-FKBP-PI-PLC-H86A to the cytosolic surface of the ER membrane in cells co-transfected with ER-localized mCherry-TM-FRB (Fig. 1, *A*, *D,* and *E*), which contains an FKBP-rapamycin binding (FRB) domain in the cytosol (8).

To selectively monitor PM PIP$_2$ replenishment in cells with PI acutely depleted at the ER membrane, cells were co-transfected with FKBP-PI-PLC and TM-FRB, a PIP$_2$ biosensor GFP-PLCδ-PH (17), and H1R to augment PIP$_2$ hydrolysis induced by histamine stimulation. In untreated (control) cells, a sharp drop in PM PLCδ-PH intensity, indicating PIP$_2$ hydrolysis, was observed using TIRF microscopy immediately following histamine stimulation. The hydrolysis was followed by an initial recovery before reaching a new steady state reflecting equilibrium between receptor-induced hydrolysis and regeneration of PIP$_2$ (Fig. 1*F*, *black line*). In cells treated with rapamycin to acutely remove PI at the ER membrane, the hydrolysis and the initial recovery of PIP$_2$ after histamine stimulation were similar to that in control cells (Fig. 1*F*, *red line*). Remarkably, the level of PIP$_2$ dropped again shortly after the initial recovery, suggesting that PI at the ER membrane supports the regeneration of PM PIP$_2$. In contrast, rapamycin treatment did not affect PIP$_2$ replenishment in cells transfected with FKBP-PI-PLC-H86A instead of FKBP-PI-PLC (Fig. 1*G*). We further employed immunostaining to detect PIP$_2$ at the PM in cells co-transfected with FKBP-PI-PLC, TM-FRB, and H1R. Consistently, we observed a significant difference in PM PIP$_2$ levels following histamine stimulation for 9 min in cells with rapamycin pretreatment as compared with control cells (Fig. 1, *H* and *I*). These results suggest that a delivery of PI from the ER to the PM occurs within minutes to support PIP$_2$ replenishment.

Disruption of PI and PI4P Delivery by Vesicular Transport Did Not Prevent the Rapid Replenishment of PM PIP$_2$—PI can be delivered from the ER to the PM indirectly via vesicular transport through the Golgi apparatus where it can be converted to PI4P before reaching the PM. To determine whether PI and PI4P delivered via vesicular transport is important for rapid PIP$_2$ replenishment, we devised another rapamycin-inducible enzymatic chimera mRFP-FKBP-Sac1-PI-PLC to selectively remove PI and PI4P at the Golgi apparatus by modifying the Pseudojanin (Fig. 2*A*) (13). Golgi localization of mRFP-FKBP-Sac1-PI-PLC and its ability to deplete PI4P at the Golgi following rapamycin treatment were observed in cells co-transfected with Tgn38-FRB-CFP for Golgi targeting and GFP-

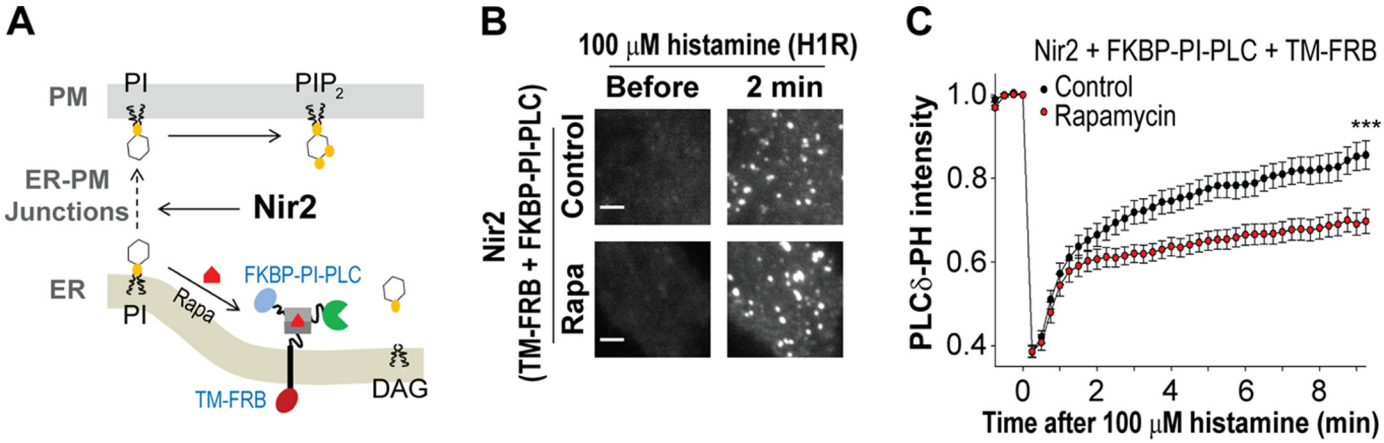

FIGURE 3. **Nir2 at ER-PM junctions mediates PM PIP_2 replenishment with PI at the ER membrane.** *A*, diagram showing experimental design to test whether Nir2 mediates inter-organelle PI transfer as indicated by a *dashed arrow*. *B*, Nir2-YFP translocation to ER-PM junctions monitored by TIRF microscopy in HeLa cells co-transfected with H1R, CFP-FKBP-PI-PLC, and mCherry-TM-FRB in the absence (control) or presence of 5 μM rapamycin (*Rapa*) pretreatment for 10 min. *Scale bar*, 2 μm. *C*, changes in PM PIP_2 levels induced by histamine in HeLa cells co-transfected with H1R, GFP-PLCδ-PH, Nir2-mCherry, CFP-FKBP-PI-PLC, and mCherry-TM-FRB in the absence (control) or presence of 5 μM rapamycin pretreatment for 10 min. Means ± S.E. are shown (30 cells from four independent experiments). ***, $p < 0.001$.

P4M for PI4P detection (Fig. 2*B*) (18, 19). Acute depletion of PI and PI4P at the Golgi by rapamycin-induced recruitment of mRFP-FKBP-Sac1-PI-PLC did not affect PM PIP_2 replenishment (Fig. 2*C*). Consistently, inhibition of ER-to-Golgi transport by brefeldin A (BFA) disrupted the Golgi apparatus but not PIP_2 replenishment (Fig. 2, *D* and *E*). In fact, BFA pretreatment resulted in a marked enhancement of PIP_2 replenishment. It is plausible that nonvesicular PI delivery compensates the inhibition of vesicular transport by BFA, leading to the enhanced PIP_2 replenishment. We have previously shown that a PITP, Nir2, promotes PM PIP_2 replenishment likely through nonvesicular pathways at ER-PM junctions (8). Nonetheless, disruption of vesicular transport by BFA pretreatment did not significantly affect receptor-induced Nir2 translocation to ER-PM junctions, as indicated by puncta formation monitored by TIRF microscopy (Fig. 2, *F* and *G*). Together with results from Fig. 1, these data suggest that the delivery of PI at the ER membrane to the PM for rapid PIP_2 replenishment is mediated by nonvesicular transport mechanisms.

PI at the ER Membrane Is Important for PIP_2 Replenishment Mediated by Nir2 at ER-PM Junctions—Next, we applied the rapamycin-inducible approach described in Fig. 1*A* to examine whether PI at the ER membrane is required for PIP_2 replenishment mediated by Nir2 at ER-PM junctions (Fig. 3*A*). Rapamycin-induced ER PI depletion did not prevent Nir2 translocation to ER-PM junctions (Fig. 3*B*). However, the enhanced PIP_2 replenishment mediated by Nir2 overexpression was significantly suppressed in rapamycin-treated cells with acute depletion of PI at the ER membrane (Fig. 3*C*). These results suggest that Nir2 mediates PIP_2 replenishment at ER-PM junctions by transferring PI at the ER membrane to the PM for the regeneration of PIP_2.

Nir2 Senses PIP_2 Hydrolysis and Translocates to ER-PM Junctions by Binding to PA—It is unclear how Nir2 senses PIP_2 hydrolysis and translocates to ER-PM junctions to mediate PIP_2 replenishment following receptor stimulation. It has been recently shown that Nir2 targets to the PM via its C-terminal LNS2 domain that binds PA produced following growth factor-induced phospholipase D activation (20). PA can be generated from DAG phosphorylation by DGK following PLC-induced PIP_2 hydrolysis (Fig. 4*A*). We hypothesize that Nir2 senses PIP_2 hydrolysis by binding to PA, which enables Nir2 translocation to ER-PM junctions. To test this hypothesis, we applied U73122 (PLC inhibitor) or R59022 (DGK inhibitor) to disrupt receptor-induced PA production (Fig. 4*A*). We found that Nir2 translocation to ER-PM junctions was inhibited in cells treated with U73122 and R59022 (Fig. 4, *B* and *C*). Remarkably, addition of exogenous PA at 400 μM was sufficient to trigger Nir2 translocation to ER-PM junctions (Fig. 4*D* and supplemental Movie S1). We further generated the Nir2-D1128A mutant (Fig. 4*E*), which disrupts the ability of Nir2 to bind PA and target to the PM (20). This mutant showed defective translocation to ER-PM junctions as compared with the wild-type Nir2 (Fig. 4, *F* and *G*). These results suggest that PA produced following PLC-mediated PIP_2 hydrolysis recruits Nir2 to ER-PM junctions by binding to the LNS2 domain of Nir2.

Disruption of Nir2 Targeting to ER-PM Junctions Inhibits PIP_2 Replenishment Mediated by Nir2—We have previously shown that the Nir2-FFAT mutant (FM) with the ER-targeting motif disrupted can translocate to the PM but cannot concentrate at ER-PM junctions, resulting in a moderate reduction in the ability to mediate PIP_2 replenishment (8). To completely prevent Nir2 targeting to ER-PM junctions, we generated the Nir2-FM-D1128A mutant (Fig. 4*E*), and we confirmed that this mutant failed to translocate to ER-PM junctions (Fig. 4*H*). Notably, the ability of Nir2 to enhance PIP_2 replenishment was abolished in the Nir2-FM-D1128A mutant, indicating that translocation to ER-PM junctions is crucial for Nir2 to mediate PIP_2 replenishment (Fig. 4*I*).

We further generated Nir2-PITP, a deletion mutant that contains only the PITP domain and fails to translocate to ER-PM junctions following stimulation because it lacks the targeting motifs for the ER and the PM (Fig. 4, *E* and *H*). Compared with cells overexpressing the full-length Nir2, cells expressing

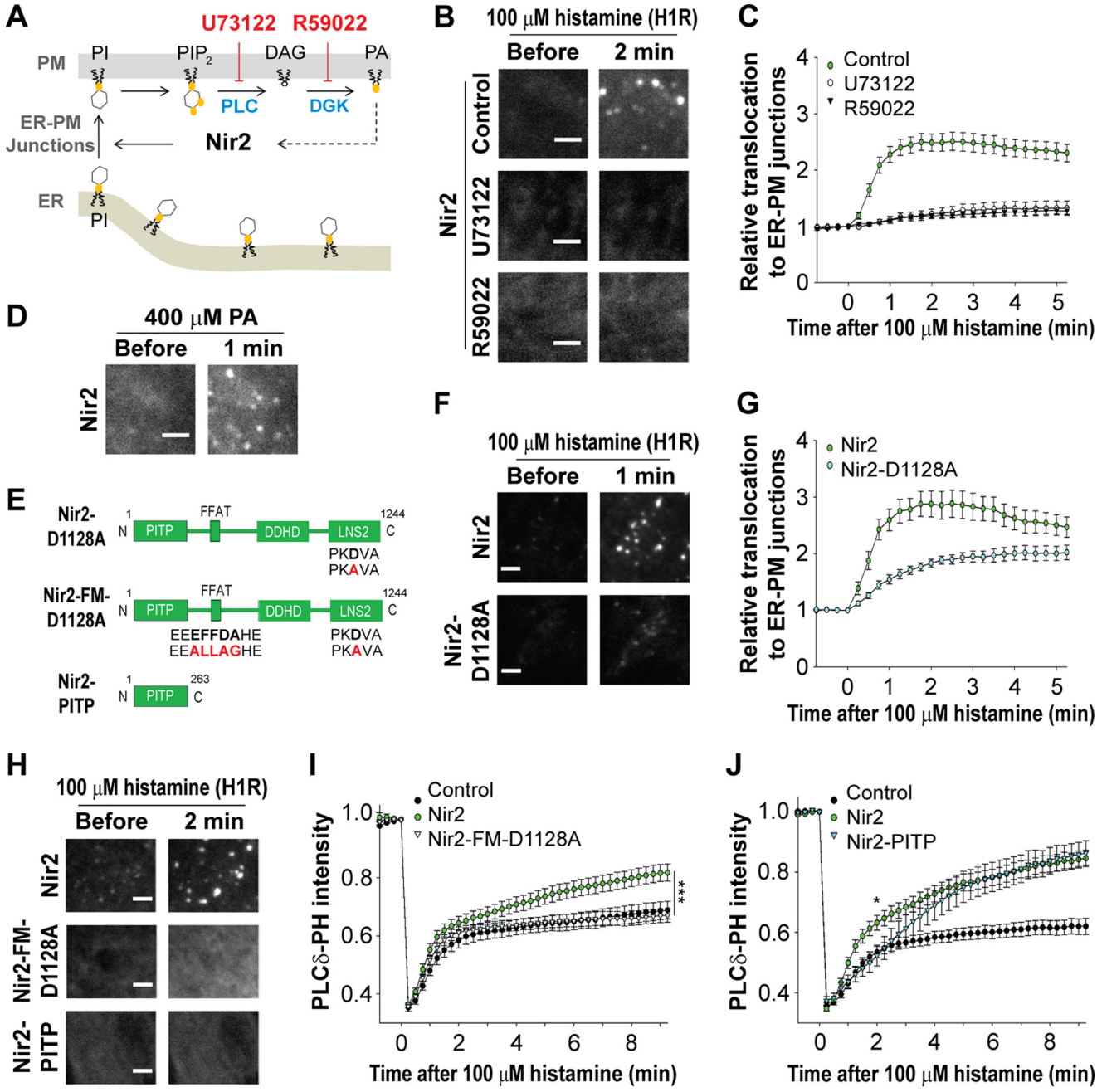

FIGURE 4. **Feedback regulation of PIP$_2$ homeostasis by Nir2 at ER-PM junctions.** *A*, diagram showing the hypothesis (*dashed arrow*) that Nir2 is a feedback regulator of PIP$_2$ homeostasis at ER-PM junctions by sensing PA production following PIP$_2$ hydrolysis. *B*, Nir2-mCherry translocation to ER-PM junctions induced by 100 μM histamine monitored by TIRF microscopy in HeLa cells transfected with H1R and pretreated with 1 μM U73122 or 25 μM R59022 for an hour. *Scale bar*, 2 μm. *C*, relative translocation of Nir2 to ER-PM junctions monitored by TIRF microscopy in HeLa cells as described in *B*. Means ± S.E. are shown (7–18 cells from at least two independent experiments). *D*, Nir2-mCherry translocation to ER-PM junctions triggered by 400 μM PA in HeLa cells monitored by TIRF microscopy. *Scale bar*, 2 μm. See also supplemental Movie S1. *E*, diagram of Nir2-D1128A mutant, Nir2-FM-D1128A mutant, and Nir2-PITP. Mutated residues are shown in *red*. Amino acid numbers and domains are indicated. *F*, changes in Nir2-mCherry and Nir2-D1128A-mCherry localization following histamine treatment monitored by TIRF microscopy in HeLa cells expressing H1R. *Scale bar*, 2 μm. *G*, translocation of Nir2-mCherry and Nir2-D1128A-mCherry to ER-PM junctions as described in *F*. Means ± S.E. are shown (seven cells from two independent experiments). *H*, changes in Nir2-mCherry, Nir2-FM-D1128A-mCherry, and Nir2-PITP-mCherry localization following histamine treatment monitored by TIRF microscopy in HeLa cells transfected with H1R. *Scale bar*, 2 μm. *I*, changes in PM PIP$_2$ levels in HeLa cells co-transfected with H1R, GFP-PLCδ-PH, and control (mCherry-N1), Nir2-mCherry, or Nir2-FM-D1128A-mCherry. Means ± S.E. are shown (20–33 cells from three independent experiments). ***, $p < 0.001$ between Nir2 and Nir2-FM-D1128A. *J*, changes in PM PIP$_2$ levels in HeLa cells co-transfected with H1R, GFP-PLCδ-PH, and control (mCherry-N1), Nir2-mCherry, or Nir2-PITP-mCherry. Means ± S.E. are shown (16–31 cells from three independent experiments). *, $p < 0.05$ between Nir2 and Nir2-PITP after histamine stimulation for 2 min.

Nir2-PITP displayed no enhancement of PIP$_2$ replenishment in the first few minutes after receptor-induced PIP$_2$ hydrolysis, and an enhanced PIP$_2$ replenishment was only detected in later time points (Fig. 4*J*). These results indicate that the PITP domain of Nir2 possesses the activity for mediating PIP$_2$ replenishment and suggest that targeting to ER-PM junctions significantly facilitates the transfer of PI at the ER membrane to the PM mediated by Nir2. Because the Nir2-FM-D1128A

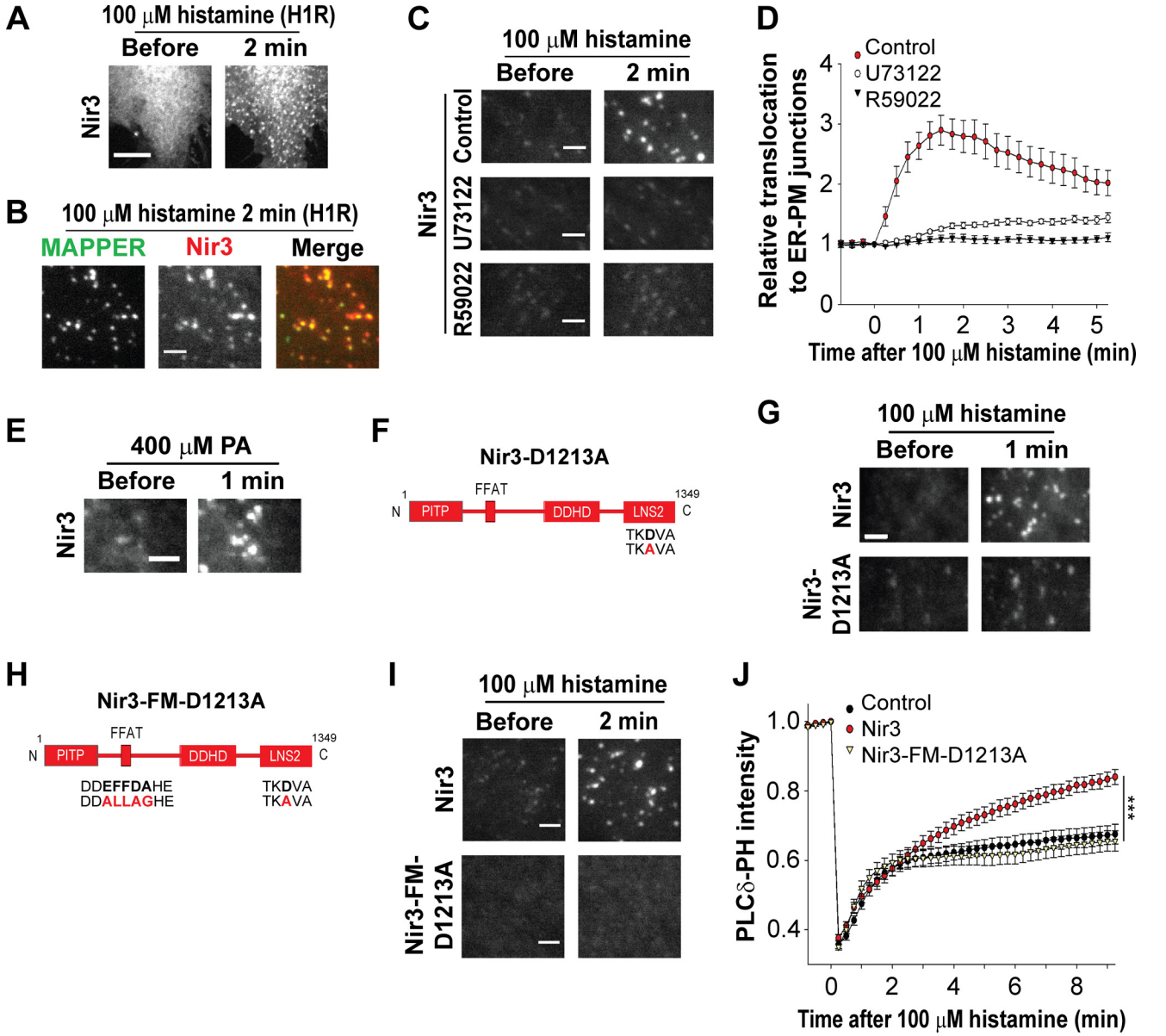

FIGURE 5. **Feedback regulation of PIP_2 homeostasis by Nir3 at ER-PM junctions.** *A,* Nir3-mCherry translocation to ER-PM junctions induced by 100 μM histamine monitored by confocal microscopy in HeLa cells transfected with H1R. *Scale bar,* 10 μm. *B,* Nir3-mCherry translocation to ER-PM junctions induced by100 μM histamine monitored by TIRF microscopy in MAPPER-expressing HeLa cells transfected with H1R. *Scale bar,* 2 μm. See also supplemental Movie S2. *C,* Nir3 translocation to ER-PM junctions induced by 100 μM histamine monitored by TIRF microscopy in HeLa cells pretreated with 1 μM U73122 or 25 μM R59022 for an hour. *Scale bar,* 2 μm. *D,* relative translocation of Nir3 to ER-PM junctions as described in *C*. Means ± S.E. are shown (7–18 cells from at least two independent experiments). *E,* Nir3-mCherry translocation to ER-PM junctions triggered by 400 μM PA in HeLa cells monitored by TIRF microscopy. *Scale bar,* 2 μm. *F,* diagram of Nir3-D1213A mutant. The mutated residue is shown in *red*. Amino acid numbers and domains are indicated. *G,* changes in Nir3-mCherry and Nir3-D1213A-mCherry localization following histamine treatment monitored by TIRF microscopy in HeLa cells. *Scale bar,* 2 μm. *H,* diagram of Nir3-FM-D1213A mutant. Mutated residues are shown in *red*. Amino acid numbers and domains are indicated. *I,* changes in Nir3-mCherry and Nir3-FM-D1213A-mCherry localization following histamine treatment monitored by TIRF microscopy in HeLa cells. *Scale bar,* 2 μm. *J,* changes in PM PIP_2 levels in HeLa cells co-transfected with H1R, GFP-PLCδ-PH, and control (mCherry-N1), Nir3-mCherry, or Nir3-FM-D1213A-mCherry. Means ± S.E. are shown, (18–21 cells are from three independent experiments.) ***, $p < 0.001$ between Nir3 and Nir3-FM-D1213A.

mutant contains an intact PITP domain but is unable to promote PIP_2 replenishment, targeting to ER-PM junctions is likely to be a key step in activating the PITP domain in the context of the full-length Nir2. In summary, the data presented in Fig. 4 suggest that Nir2 functions as a feedback regulator of PIP_2 homeostasis by sensing PA produced following PIP_2 hydrolysis and translocating to ER-PM junctions to mediate transfer of PI at the ER membrane to the PM for PIP_2 replenishment (Fig. 4*A*).

Nir3, a Homolog of Nir2, Also Translocates to ER-PM Junctions and Mediates PIP_2 Replenishment—Nir3 is a homolog of Nir2 that is expressed in many human tissues (21), but its functions are not well characterized. We found that mCherry-tagged Nir3 is localized in the cytosol and translocates to puncta following histamine stimulation (Fig. 5*A* and supplemental Movie S2). These Nir3 puncta correspond to ER-PM junctions labeled by MAPPER (Fig. 5*B*), a genetically encoded marker for ER-PM junctions (8). Consistent with Nir2,

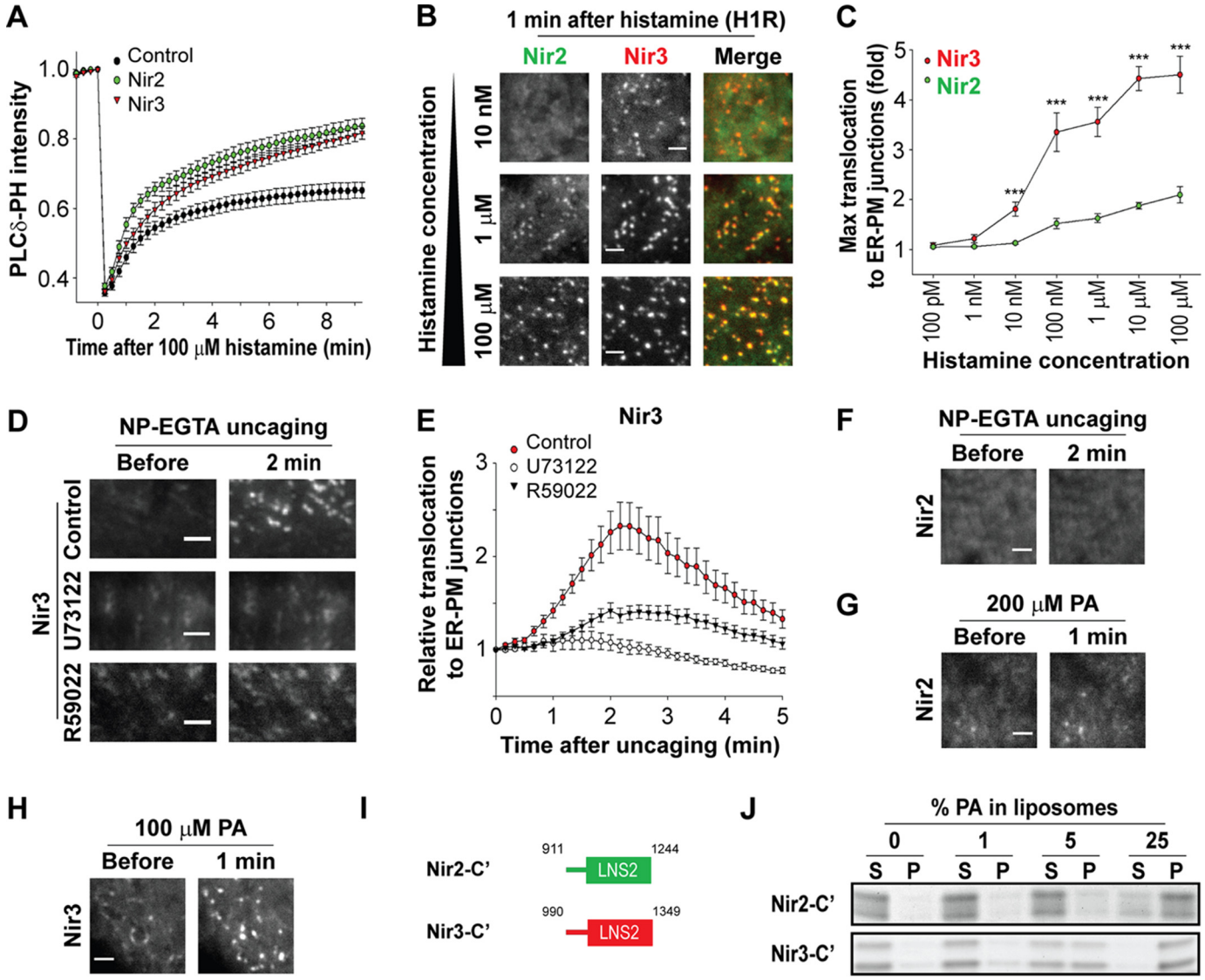

FIGURE 6. **Nir3 is more sensitive to PA production than Nir2.** *A*, changes in PM PIP$_2$ levels in HeLa cells co-transfected with H1R, GFP-PLCδ-PH, and control (mCherry-N1), Nir2-mCherry, or Nir3-mCherry. Means ± S.E. are shown (45–49 cells from at least seven independent experiments). *B*, Nir2-YFP and Nir3-mCherry translocation to ER-PM junctions induced by different concentrations of histamine monitored by TIRF microscopy in HeLa cells transfected with H1R. *Scale bar*, 2 μm. *C*, quantification of maximal Nir2-YFP or Nir3-mCherry translocation to ER-PM junctions monitored by TIRF microscopy in HeLa cells transfected with H1R. Means ± S.E. are shown (4–17 cells from at least two independent experiments). ***, $p < 0.001$. *D*, Nir3-mCherry translocation to ER-PM junctions induced by NP-EGTA uncaging monitored by TIRF microscopy in HeLa pretreated with 1 μM U73122 or 25 μM R59022 for an hour. *Scale bar*, 2 μm. *E*, quantification of relative translocation of Nir3 to ER-PM junctions monitored as described in *D*. Means ± S.E. are shown (6–15 cells from three independent experiments). *F*, Nir2-mCherry localization remains unchanged following NP-EGTA uncaging monitored by TIRF microscopy in HeLa cells loaded with NP-EGTA. *Scale bar*, 2 μm. *G*, Nir2-mCherry translocation to ER-PM junctions induced by 200 μM PA in HeLa cells monitored by TIRF microscopy. *Scale bar*, 2 μm. *H*, Nir3-mCherry translocation to ER-PM junctions induced by 100 μM PA in HeLa cells monitored by TIRF microscopy. *Scale bar*, 2 μm. See also supplemental Movie S3. *I*, diagram of the C-terminal regions of Nir2 (*Nir2-C′*) and Nir3 (*Nir3-C′*). Amino acid numbers and LNS2 domain are indicated. *J*, differential binding of Nir2-C′ and Nir3-C′ to PA assessed by liposome sedimentation assay with liposome consisting of PC alone (0%) or PC plus indicated percentage of PA. *S* and *P* indicate supernatant and pellet, respectively. Representative SDS-PAGE images are shown (three independent experiments).

Nir3 translocation to ER-PM junctions was inhibited by U73122 or R59022 (Fig. 5, *C* and *D*). Addition of exogenous PA at 400 μM was sufficient to trigger the translocation of Nir3 to ER-PM junctions (Fig. 5*E*). Moreover, the Nir3-D1213A mutant that contains the corresponding mutation to the key PA-binding residue in Nir2 exhibited reduced translocation to ER-PM junctions (Fig. 5, *F* and *G*). The Nir3-FM-D1213A mutant with both the ER- and the PM-targeting motifs disrupted failed to translocate to ER-PM junctions or enhance PIP$_2$ replenishment as compared with the wild-type Nir3 (Fig. 5, *H–J*). Together, these results indicate that Nir3, in addition to Nir2, is a feedback regulator of PIP$_2$ homeostasis.

Nir3 Is More Sensitive to PA Production than Nir2 and Translocates to ER-PM Junctions Independently—We noted that Nir3-overexpressing cells exhibited a slower initial replenishment of PIP$_2$ than Nir2-overexpressing cells (Fig. 6*A*), suggesting that Nir3 is less active in replenishing PIP$_2$ than Nir2. We postulated that the less potent PIP$_2$ replenishment by Nir3 is due to a weaker translocation to ER-PM junctions. Surprisingly, the translocation of Nir3, but not Nir2, to ER-PM junctions was

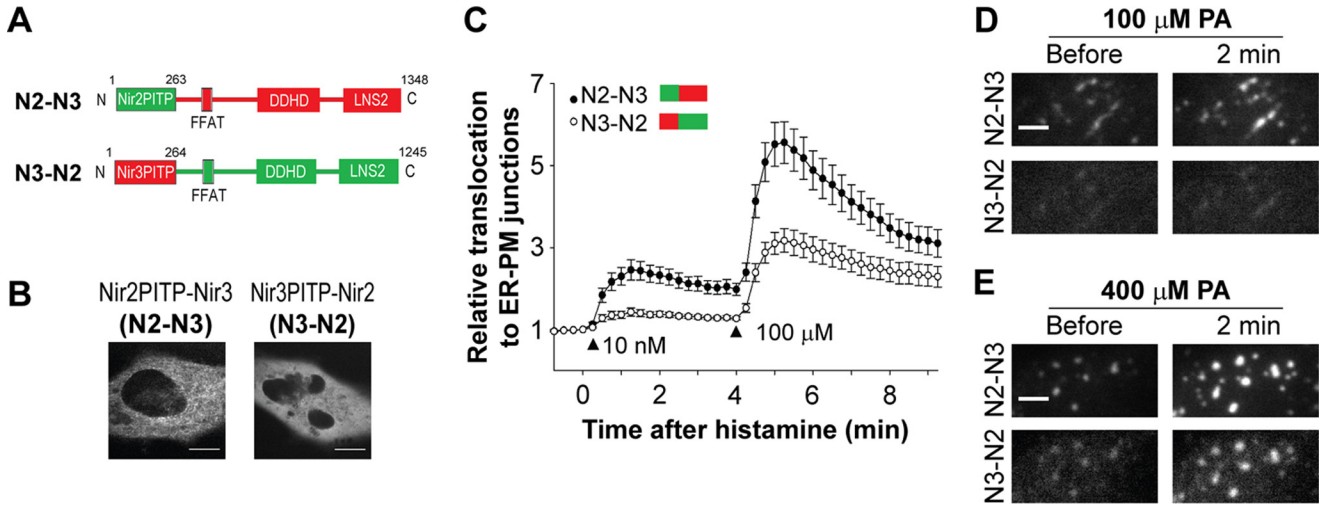

FIGURE 7. **C-terminal regions of Nir2 and Nir3 determine the extent of their translocation to ER-PM junctions.** *A*, diagrams of Nir2PITP-Nir3 (*N2-N3*) and Nir3PITP-Nir2 (*N3-N2*) chimeras. Amino acid numbers and domains are indicated. *B*, Nir2PITP-Nir3 (*N2-N3*) and Nir3PITP-Nir2 (*N3-N2*) show cytosolic localization in HeLa cells monitored by confocal microscopy. *Scale bar*, 10 μm. *C*, relative translocation of N2-N3 and N3-N2 to ER-PM junctions monitored by TIRF microscopy in HeLa cells co-transfected with H1R. Means ± S.E. are shown (13–15 cells from two to three independent experiments). See also supplemental Movie S4. *D* and *E*, N2-N3-mCherry and N3-N2-YFP translocation to ER-PM junctions induced by 100 μM PA (*D*) or 400 μM PA (*E*) monitored by TIRF microscopy in HeLa cells. *Scale bar*, 2 μm.

readily detected following 10 nM histamine stimulation in cells co-transfected with Nir2-YFP, Nir3-mCherry, and H1R (Fig. 6*B*, *top panels*). In these cells, Nir2 appeared at ER-PM junctions after 1 and 100 μM histamine stimulation, although substantial accumulation of Nir3 was observed at the same junctions (Fig. 6*B*, *middle* and *bottom panels*). The maximal translocation of Nir3 to ER-PM junctions was significantly higher than that of Nir2 in cells stimulated with histamine ranging from 10 nM to 100 μM (Fig. 5*C*). These results suggest that Nir3 translocation to ER-PM junctions occurs following low levels of receptor activation, whereas Nir2 translocation requires intense receptor stimulation.

To further demonstrate that Nir3 can sense low levels of PIP_2 hydrolysis, we used NP-EGTA, a caged Ca^{2+} reagent that releases chelated Ca^{2+} to the cytosol upon UV illumination to trigger a transient activation of PLC. Uncaging of NP-EGTA triggered Nir3 but not Nir2 translocation to ER-PM junctions (Fig. 6, *D* and *F*). This translocation was suppressed in cells pretreated with U73122 or R59022, suggesting that Ca^{2+}-induced Nir3 translocation was mediated by PA production from PLC-induced PIP_2 hydrolysis (Fig. 6, *D* and *E*). In addition, Nir2 translocation was barely detectable following treatment of 200 μM PA (Fig. 6*G*), whereas Nir3 translocation was apparent in cells treated with 100 μM of PA (Fig. 6*H*; supplemental Movie S3). These data indicate that Nir3 is more sensitive to PA production than Nir2 and that Nir3 independently translocates to ER-PM junctions in response to a slight activation of PIP_2 hydrolysis.

C-terminal Region Determines the Ability of Nir2 and Nir3 to Bind PA and Translocate to ER-PM Junctions—To more directly demonstrate the differential PA binding abilities of Nir2 and Nir3, we performed liposome sedimentation assays using recombinant proteins of the C-terminal regions of Nir2 (Nir2-C′) and Nir3 (Nir3-C′) (Fig. 6*I*). Consistent with the results from a recent study (20), a clear shift of Nir2-C′ from the supernatants to the pellets, indicating its binding to liposomes, was observed with liposomes containing 25% but not 5 or 1% PA. However, a clear shift of Nir3-C′ from the supernatants to the pellets was readily detected with liposomes containing 5% PA, and a nearly complete shift was observed with liposomes containing 25% PA. These results support that the Nir3 has a higher PA-binding ability than Nir2. Given that Nir2 harbors a C-terminal region with a lower PA-binding ability and translocates to ER-PM junctions to a lesser extent than Nir3 following receptor stimulation (Fig. 6*C*), the more potent PIP_2 replenishment mediated by Nir2 (Fig. 6*A*) is likely due to a higher activity of its PITP domain. To test this idea, we generated chimeras with the PITP domain swapped between Nir2 and Nir3 (Fig. 7*A*). Both chimeras, Nir2PITP-Nir3 (N2-N3) and Nir3PITP-Nir2 (N3-N2), showed cytosolic localization when expressed in HeLa cells (Fig. 7*B*). Similar to Nir3, N2-N3 translocated to ER-PM junctions after 10 nM histamine stimulation (Fig. 7*C*; supplemental Movie S4). Moreover, translocation of N3-N2, resembling that of Nir2, was only observed following 100 μM histamine treatment accompanied by additional N2-N3 accumulation at ER-PM junctions. Consistently, 100 μM PA was sufficient to trigger N2-N3, but not N3-N2, translocation in cells co-transfected with both chimeras (Fig. 7*D*). After 400 μM PA treatment, a discernible N3-N2 translocation was detected accompanied by a greater accumulation of N2-N3 at the same ER-PM junctions (Fig. 7*E*). These results indicate that the C-terminal region containing the ER- and the PM-targeting motifs, but not the N-terminal PITP domain, determines the extent of translocation of Nir2, Nir3, and the chimeras following receptor activation.

PITP Domain of Nir2 Has a Higher Activity than That of Nir3 in Mediating PIP_2 Replenishment—To compare the activity of the PITP domains of Nir2 and Nir3 in mediating PIP_2 replenishment, we performed experiments using protein pairs with the same C-terminal region and the ability to translocate to ER-PM junctions. Despite the comparable

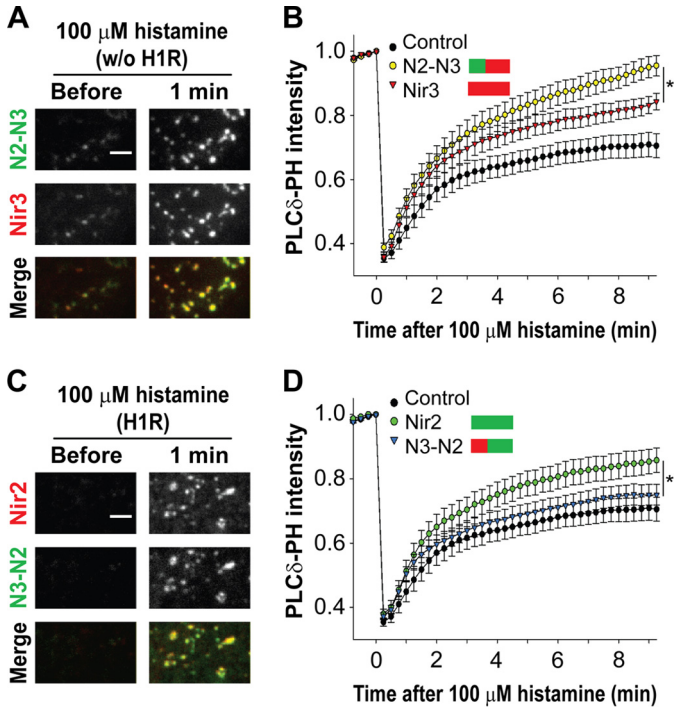

FIGURE 8. **PITP domain of Nir2 is more potent in mediating PIP$_2$ replenishment than that of Nir3.** *A,* translocation of Nir3-mCherry and N2-N3-YFP to ER-PM junctions monitored by TIRF microscopy in HeLa cells. *Scale bar,* 2 μm. *B,* changes in PM PIP$_2$ levels induced by histamine monitored in HeLa cells co-transfected with H1R, GFP-PLCδ-PH, and control (mCherry-N1), N2-N3-mCherry, or Nir3-mCherry. Means ± S.E. are shown (18–32 cells from three independent experiments). *, $p < 0.05$ between N2-N3 and Nir3. *C,* translocation of Nir2-mCherry and N3-N2-YFP to ER-PM junctions monitored by TIRF microscopy in HeLa cells expressing H1R. *Scale bar,* 2 μm. *D,* changes in PM PIP$_2$ levels induced by histamine monitored in HeLa cells co-transfected with H1R, GFP-PLCδ-PH, and control (mCherry-N1), Nir2-mCherry, or N3-N2-mCherry. Means ± S.E. are shown (18–28 cells from three independent experiments). *, $p < 0.05$ between Nir2 and N3-N2.

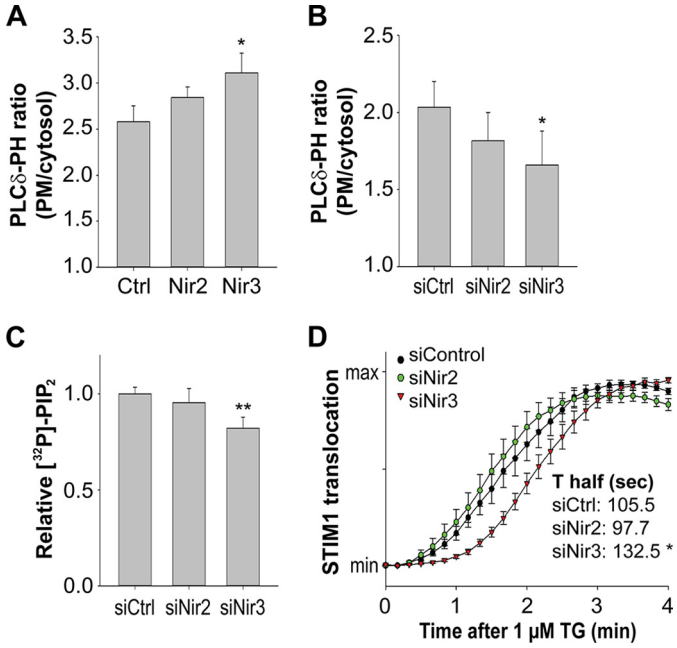

FIGURE 9. **Nir3 is important for maintaining basal PM PIP$_2$ levels.** *A,* basal PM PIP$_2$ levels monitored in HeLa cells co-transfected with GFP-PLCδ-PH and control (*Ctrl,* mCherry-N1), Nir2-mCherry, or Nir3-mCherry. Mean ± S.D. are shown (three independent experiments). *, $p < 0.05$ as compared with control. *B,* basal PM PIP$_2$ level monitored in HeLa cells co-transfected with GFP-PLCδ-PH and siControl (*siCtrl*), siNir2, or siNir3. Mean ± S.D. are shown (five independent experiments). *, $p < 0.05$ as compared with control. *C,* basal PM PIP$_2$ level monitored by [^{32}P]phosphate labeling in HeLa cells transfected with siControl (*siCtrl*), siNir2, or siNir3. Mean ± S.D. are shown (four replicates from two independent experiments). **, $p < 0.01$ as compared with control. *D,* relative YFP-STIM1 translocation to ER-PM junctions following thapsigargin (*TG*) monitored by TIRF microscopy in HeLa cells transfected with siControl, siNir2, or siNir3. Means ± S.E. are shown (10–13 cells from three independent experiments). Mean times to the half-maximal translocation (*T half*) are indicated. *, $p < 0.05$ as compared with siControl (*siCtrl*).

translocation of N2-N3 and Nir3 to ER-PM junctions following receptor stimulation in co-transfected cells (Fig. 8*A*), PIP$_2$ replenishment mediated by N2-N3 was significantly enhanced relative to that mediated by Nir3 (Fig. 8*B*). These results suggest that the Nir2 PITP domain has a higher activity in mediating PIP$_2$ replenishment than that of Nir3. We further compared PIP$_2$ replenishment mediated by N3-N2 and Nir2, both of which translocate to ER-PM junctions in a similar manner following receptor stimulation in cells co-transfected with H1R (Fig. 8*C*). PIP$_2$ replenishment mediated by N3-N2 was significantly reduced compared with that mediated by Nir2 (Fig. 8*D*). Together, these results indicate that the PITP domain and the C-terminal region of Nir2 and Nir3 can function as independent modules and that the PITP domain of Nir2 has a higher activity in mediating PIP$_2$ replenishment than that of Nir3.

Nir3 Is Important for Maintaining Basal PM PIP$_2$ Levels—The high sensitivity to PIP$_2$ hydrolysis and the less active PITP domain of Nir3 prompted us to postulate that Nir3 contributes to maintaining basal PM PIP$_2$ levels. We tested this hypothesis by using confocal microscopy to monitor the ratio of PLCδ-PH intensity at the PM to that in the cytosol as an indicator of PM PIP$_2$ levels. We found that Nir3 overexpression resulted in a significant elevation of basal PM PIP$_2$ levels in cells, whereas treatment using siRNA targeting Nir3 (siNir3) had an opposite effect (Fig. 9, *A* and *B*). Similarly, only siNir3-treated cells exhibited a significant decrease in basal PIP$_2$ levels as demonstrated by [^{32}P]phosphate metabolic labeling experiments (Fig. 9*C*). The contribution of Nir2 to basal PM PIP$_2$ levels was not significant (Fig. 9, *A*–*C*). PM PIP$_2$ binding via a C-terminal polybasic motif facilitates the translocation of the ER Ca^{2+} sensor STIM1 to ER-PM junctions (3, 22). Consistent with a role of Nir3 in maintaining PM PIP$_2$ levels in cells without receptor stimulation, STIM1 translocation to ER-PM junctions induced by the ER Ca^{2+}-ATPase inhibitor thapsigargin was significantly delayed in siNir3- but not siNir2-treated cells (Fig. 9*D*).

Nir3 Is the Major PITP That Maintains PM PIP$_2$ Homeostasis during Low Levels of Receptor Activation—We further examined the roles of Nir2 and Nir3 in PIP$_2$ replenishment induced by a low level of receptor activation using 1 μM instead of 100 μM histamine. In siControl-transfected cells, stimulation with 1 μM histamine led to an 85% PM PIP$_2$ recovery (Fig. 10*A*), higher than the 60–70% recovery observed in control cells from previous experiments with 100 μM histamine stimulation (Fig. 6*A*, for example). A significant reduction in PIP$_2$ replenishment, as monitored by PIP$_2$ biosensor, following stimulation of 1 μM histamine was detected in siNir3-treated cells, although a moderate effect was observed in siNir2-treated cells. Similarly, we

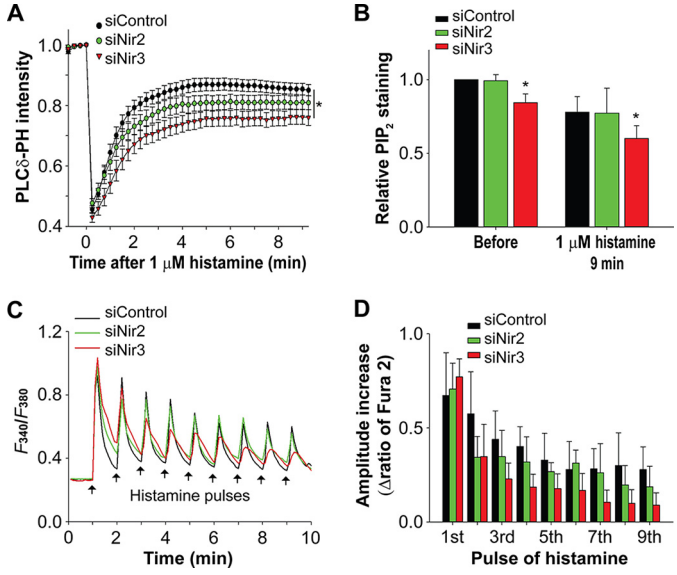

FIGURE 10. **Nir3 is the major PITP that maintains PM PIP$_2$ homeostasis during low levels of receptor activation.** *A,* changes in PM PIP$_2$ levels induced by 1 μM histamine treatment of HeLa cells co-transfected with H1R, GFP-PLCδ-PH, and siControl, siNir2, or siNir3. Means ± S.E. are shown (22–24 cells from four independent experiments). *, $p < 0.05$. *B,* relative PM PIP$_2$ levels monitored by PIP$_2$ immunostaining in HeLa cells co-transfected with H1R, and siControl, siNir2, or siNir3 before or 9 min after 1 μM histamine treatment. Mean ± S.D. are shown (three independent experiments). *, $p < 0.05$ as compared with siControl. *C,* relative changes in cytosolic Ca^{2+} concentration monitored by Fura-2 ratio in HeLa cells transfected with siControl, siNir2, or siNir3. Cells were subjected to multiple pulses of 100 μM histamine (*arrows*) in a perfusion system. Average traces are shown (four to five wells from three independent experiments). *D,* quantification of amplitude increases of each pulse from data shown in *C*. Mean ± S.D. is shown.

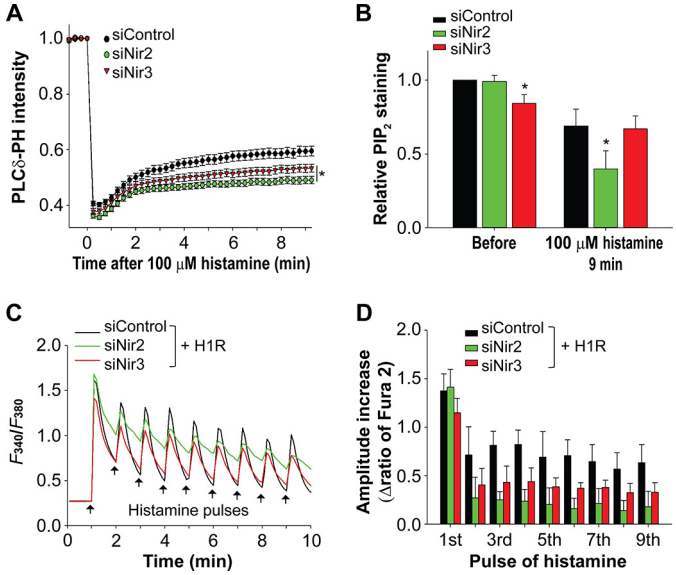

FIGURE 11. **Nir2 is more important than Nir3 in maintaining PM PIP$_2$ homeostasis during intense receptor activation.** *A,* changes in PM PIP$_2$ levels induced by 100 μM histamine treatment of HeLa cells co-transfected with H1R, GFP-PLCδ-PH, and siControl, siNir2, or siNir3. Means ± S.E. are shown (35–42 cells from at least five independent experiments). *, $p < 0.05$. *B,* relative PM PIP$_2$ levels monitored by PIP$_2$ immunostaining in HeLa cells co-transfected with H1R, and siControl, siNir2, or siNir3 before or 9 min after 100 μM histamine treatment. Means ± S.D. are shown (three independent experiments). *, $p < 0.05$ as compared with siControl. *C,* relative changes in cytosolic Ca^{2+} concentration monitored by Fura-2 ratio in HeLa cells co-transfected with H1R and siControl, siNir2, or siNir3. Cells were subjected to multiple pulses of 100 μM histamine (*arrows*) in a perfusion system. Average traces are shown (four to eight wells from at least three independent experiments). *D,* quantification of amplitude increases of each pulse from data shown in *C*. Mean ± S.D. is shown.

observed a significant decrease in PM PIP$_2$ levels 9 min after 1 μM histamine stimulation in siNir3-treated cells using PIP$_2$ immunostaining (Fig. 10*B*). In addition, PIP$_2$ immunostaining also revealed a reduction in basal PIP$_2$ levels in siNir3-transfected cells. These results suggest that Nir3 is more important in replenishing PIP$_2$ hydrolyzed by a low level of receptor activation.

Moreover, we monitored the changes in cytosolic Ca^{2+} levels triggered by receptor-induced PIP$_2$ hydrolysis in cells without overexpressing H1R and periodically stimulated with a brief pulse of histamine in a cell perfusion system. We observed that the first pulse of histamine stimulation triggered comparable cytosolic Ca^{2+} increases in siControl-, siNir2-, and siNir3-transfected cells (Fig. 10, *C* and *D*). Notably, a profound decrease in the amplitude of Ca^{2+} responses to subsequent pulses of histamine stimulation was observed in siNir3-transfected cells, although siNir2 treatment showed a lesser effect. These results support that Nir3 is the major PITP that contributes to PIP$_2$ replenishment during low levels of receptor activation.

Nir2 Is More Important than Nir3 in Maintaining PM PIP$_2$ Homeostasis during Intense Receptor Activation—Next, we examined the differential roles of Nir2 and Nir3 in regulating PIP$_2$ homeostasis and cell signaling during intense receptor activation. We found that siNir2-transfected cells showed a more significant defect in PIP$_2$ replenishment, as demonstrated by PIP$_2$ biosensor and PIP$_2$ immunostaining, following 100 μM histamine stimulation than siNir3-transfected cells (Fig. 11, *A* and *B*). Consistently, a more severe defect in Ca^{2+} signaling triggered by periodic stimulation with 100 μM histamine was observed in cells treated with siNir2 rather than siNir3 with a background of H1R overexpression to resemble intense receptor activation (Fig. 11, *C* and *D*). These results demonstrate a more important role of Nir2 than Nir3 in cell signaling during intense receptor activation. Notably, relatively more sustained Ca^{2+} levels were detected during the washout phases in siNir2-treated cells (Fig. 11*C*), suggesting that the Ca^{2+} clearance machinery was affected by siNir2 treatment. Given that PM Ca^{2+}-ATPases are positively regulated by PIP$_2$ levels (23), the sustained cytosolic Ca^{2+} levels may reflect a reduction in PM Ca^{2+}-ATPase activities due to defective replenishment of PM PIP$_2$ in siNir2-treated cells. In summary, our data reveal the distinct roles of Nir2 and Nir3 in regulating PIP$_2$ homeostasis in cells in different physiological states.

Discussion

Our findings reveal molecular mechanisms that connect PIP$_2$ hydrolysis at the PM to its replenishment mediated by the feedback regulators Nir2 and Nir3 at ER-PM junctions (Fig. 12). We propose that, in the resting state, small amounts of PA generated by spontaneous receptor fluctuations recruit Nir3 to ER-PM junctions to mediate PI transfer from the ER to the PM to maintain basal PIP$_2$ levels. Intense receptor stimulation triggers a sizable production of PA, resulting in the translocation of

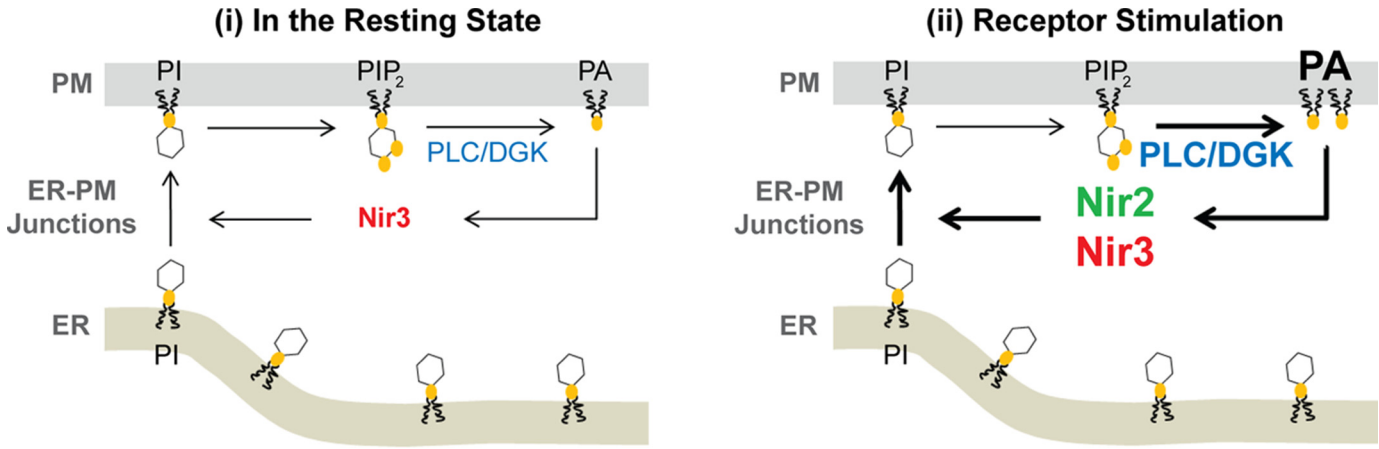

FIGURE 12. **Model for feedback regulation of PIP_2 homeostasis mediated by Nir2 and Nir3 in different physiological states.**

the more potent PITP Nir2, as well as Nir3, to ER-PM junctions to supply the PM with a substantial amount of PI needed for PIP_2 replenishment.

We demonstrate that PI at the ER membrane but not PI4P/PI at the Golgi apparatus is important for the rapid replenishment of PIP_2 following receptor-induced hydrolysis by devising enzymatic chimeras to acutely manipulate different pools of PIP_2 precursors while minimizing perturbations to the cells. These results are consistent with recent studies showing that constitutive depletion of PI at the ER membrane results in defective PIP_2 replenishment and that PI4P at the Golgi apparatus or vesicular transport is dispensable for PIP_2 replenishment (5, 12, 19). It is noteworthy that we observed an initial recovery of PM PIP_2 levels occurring within the 1st min after receptor-induced hydrolysis in cells, which was not affected by the acute depletion of PIP_2 precursors at the ER or Golgi. Thus, this initial recovery likely reflects PIP_2 regeneration from a limited pool of precursors at the PM. This observation is consistent with previous findings in cardiac myocytes predicting that following PLC-mediated hydrolysis, PIP_2 is regenerated from a limited pool of PI at the PM just a few times greater than the initial pool of PM PIP_2 (24). Together, these data indicate that PIP_2 precursors at the PM are limited and that transfer of ER PI to the PM quickly following receptor activation is essential to support PIP_2 replenishment.

Nonvesicular PI transfer via PITPs at ER-PM junctions is postulated to deliver PI from the ER to the PM (4, 25). By combining a rapamycin-inducible ER PI-depleting approach with Nir2 overexpression, we provide evidence of a PITP-mediating inter-organelle PI transfer in intact cells. It has also been suggested that PITPs may function by presenting PI to its kinases or positively regulating these kinases (26, 27). Further investigations are needed to test whether Nir2 and Nir3 work in concert with PI kinases to ensure a rapid generation of PIP_2 from PI. A recent study proposed that PI could be delivered to the PM by ER-derived PI-synthesizing compartments that make repetitive contacts with other organelles (12). Because these contacts are not exclusive to the PM, this could be a housekeeping mechanism that constantly provides PI to other membranes in the resting state. We further demonstrate that Nir2 and Nir3 act as sensors for PIP_2 hydrolysis via PA binding, which is consistent with a previous study showing that Nir2 binds PA via its LNS2 domain and translocates to the PM (20). In addition, we define the PM microdomains, namely ER-PM junctions, where Nir2 and Nir3 specifically target to mediate inter-organelle lipid transfer based on the metabolic needs of the cell. Combined with the data showing that Nir2 promotes PIP_2 replenishment with PI at the ER membrane, we reveal a novel feedback mechanism for PIP_2 homeostasis.

Using chimeras of Nir2 and Nir3, we demonstrate that the PITP domain of Nir2 is more capable of mediating PIP_2 replenishment than that of Nir3. These data are consistent with previous findings showing that reconstitution of Nir2, but not Nir3, in *Drosophila* RdgB mutants fully rescues the defects in photoreceptor cells under continuous light exposure (27). In addition, Nir2-deficient mice showed embryonic lethality indicating the importance of Nir2 during development, whereas mice lacking Nir3 appeared to be fertile and healthy (28). Nonetheless, a recent study demonstrated that Nir2 knock-out mice are viable and fertile (29). Further studies in these animals are needed to resolve the controversy and might shed light on the physiological significance of Nir2 and Nir3.

We also found that Nir2 has a reduced ability to sense PA compared with Nir3, which is consistent with our previous finding that Nir2 translocation is greatly enhanced in cells overexpressing H1R (8). Because Nir2 contains a PITP domain with a stronger PIP_2-replenishing ability, its weak translocation to ER-PM junctions following receptor stimulation may provide a mechanism to prevent overshoot of PM PIP_2 levels. By contrast, the high PA sensitivity underlies the important role of Nir3 in maintaining basal PIP_2 homeostasis. This elaborate design enables two protein homologs to differentially regulate a cellular process under distinct physiological states using the same activation mechanisms. This design principle has been repeatedly exploited in evolution as exemplified by the STIM1 and STIM2 regulation of SOCE, a feedback mechanism for maintaining ER Ca^{2+} levels following PIP_2 hydrolysis-triggered ER Ca^{2+} release (30). Intriguingly, STIM1 and STIM2 also function at ER-PM junctions to differentially regulate SOCE in cells during receptor stimulation and in the resting state, respectively. These findings indicate a pivotal role of ER-PM junctions in feedback regulation of PM PIP_2 and ER Ca^{2+} levels and sug-

gest a cross-talk between PIP_2 homeostasis and Ca^{2+} signaling at ER-PM junctions.

Acknowledgments—We thank Dr. Joseph Albanesi and Dr. Barbara Barylko for providing suggestions and technical assistance for the [^{32}P]phosphate labeling experiment. We are grateful to Dr. Tamas Balla for providing PI-PLC, PI-PLC-H86A, Tgn38-FRB-CFP, and GFP-PKD-C1ab plasmids; Dr. Gerald Hammond for providing Pseudojanin and GFP-P4M plasmids; Dr. Tobias Meyer for providing GFP-PLCδ-PH, YFP-Golgi, and CFP-FKBP-INP54 plasmids; Dr. Elliott Ross for providing histamine H1 receptor plasmid; and Linda Patterson for administrative assistance. We thank Drs. James Stull, Donald Hilgemann, and Ilya Bezprozvanny for comments on the manuscript. We are grateful to Yeeling Lam and Yi-Chun Kuo for the assistance for protein purification.

References

1. Balla, T. (2013) Phosphoinositides: tiny lipids with giant impact on cell regulation. *Physiol. Rev.* **93,** 1019–1137
2. Di Paolo, G., and De Camilli, P. (2006) Phosphoinositides in cell regulation and membrane dynamics. *Nature* **443,** 651–657
3. Nakatsu, F., Baskin, J. M., Chung, J., Tanner, L. B., Shui, G., Lee, S. Y., Pirruccello, M., Hao, M., Ingolia, N. T., Wenk, M. R., and De Camilli, P. (2012) PtdIns4P synthesis by PI4KIIIα at the plasma membrane and its impact on plasma membrane identity. *J. Cell Biol.* **199,** 1003–1016
4. Lev, S. (2012) Nonvesicular lipid transfer from the endoplasmic reticulum. *Cold Spring Harb. Perspect. Biol.* **4,** a013300
5. Dickson, E. J., Jensen, J. B., and Hille, B. (2014) Golgi and plasma membrane pools of PI(4)P contribute to plasma membrane PI(4,5)P2 and maintenance of KCNQ2/3 ion channel current. *Proc. Natl. Acad. Sci. U.S.A.* **111,** E2281–E2290
6. Shulga, Y. V., Topham, M. K., and Epand, R. M. (2011) Regulation and functions of diacylglycerol kinases. *Chem. Rev.* **111,** 6186–6208
7. Creba, J. A., Downes, C. P., Hawkins, P. T., Brewster, G., Michell, R. H., and Kirk, C. J. (1983) Rapid breakdown of phosphatidylinositol 4-phosphate and phosphatidylinositol 4,5-bisphosphate in rat hepatocytes stimulated by vasopressin and other Ca^{2+}-mobilizing hormones. *Biochem. J.* **212,** 733–747
8. Chang, C. L., Hsieh, T. S., Yang, T. T., Rothberg, K. G., Azizoglu, D. B., Volk, E., Liao, J. C., and Liou, J. (2013) Feedback regulation of receptor-induced Ca^{2+} signaling mediated by E-Syt1 and Nir2 at endoplasmic reticulum-plasma membrane junctions. *Cell Rep.* **5,** 813–825
9. Garner, K., Hunt, A. N., Koster, G., Somerharju, P., Groves, E., Li, M., Raghu, P., Holic, R., and Cockcroft, S. (2012) Phosphatidylinositol transfer protein, cytoplasmic 1 (PITPNC1) binds and transfers phosphatidic acid. *J. Biol. Chem.* **287,** 32263–32276
10. Liou, J., Kim, M. L., Heo, W. D., Jones, J. T., Myers, J. W., Ferrell, J. E., Jr., and Meyer, T. (2005) STIM is a Ca^{2+} sensor essential for Ca^{2+}-store-depletion-triggered Ca^{2+} influx. *Curr. Biol.* **15,** 1235–1241
11. Suh, B. C., Inoue, T., Meyer, T., and Hille, B. (2006) Rapid chemically induced changes of PtdIns(4,5)P2 gate KCNQ ion channels. *Science* **314,** 1454–1457
12. Kim, Y. J., Guzman-Hernandez, M. L., and Balla, T. (2011) A highly dynamic ER-derived phosphatidylinositol-synthesizing organelle supplies phosphoinositides to cellular membranes. *Dev. Cell* **21,** 813–824
13. Hammond, G. R., Fischer, M. J., Anderson, K. E., Holdich, J., Koteci, A., Balla, T., and Irvine, R. F. (2012) PI4P and PI(4,5)P2 are essential but independent lipid determinants of membrane identity. *Science* **337,** 727–730
14. Edelstein, A., Amodaj, N., Hoover, K., Vale, R., and Stuurman, N. (2010) Computer control of microscopes using microManager. *Curr. Protoc. Mol. Biol.* Chapter 14, Unit 14.20
15. Hammond, G. R., Schiavo, G., and Irvine, R. F. (2009) Immunocytochemical techniques reveal multiple, distinct cellular pools of PtdIns4P and PtdIns(4,5)P(2). *Biochem. J.* **422,** 23–35
16. Barylko, B., Gerber, S. H., Binns, D. D., Grichine, N., Khvotchev, M., Südhof, T. C., and Albanesi, J. P. (2001) A novel family of phosphatidylinositol 4-kinases conserved from yeast to humans. *J. Biol. Chem.* **276,** 7705–7708
17. Stauffer, T. P., Ahn, S., and Meyer, T. (1998) Receptor-induced transient reduction in plasma membrane PtdIns(4,5)P2 concentration monitored in living cells. *Curr. Biol.* **8,** 343–346
18. Hammond, G. R., Machner, M. P., and Balla, T. (2014) A novel probe for phosphatidylinositol 4-phosphate reveals multiple pools beyond the Golgi. *J. Cell Biol.* **205,** 113–126
19. Szentpetery, Z., Várnai, P., and Balla, T. (2010) Acute manipulation of Golgi phosphoinositides to assess their importance in cellular trafficking and signaling. *Proc. Natl. Acad. Sci. U.S.A.* **107,** 8225–8230
20. Kim, S., Kedan, A., Marom, M., Gavert, N., Keinan, O., Selitrennik, M., Laufman, O., and Lev, S. (2013) The phosphatidylinositol-transfer protein Nir2 binds phosphatidic acid and positively regulates phosphoinositide signalling. *EMBO Rep.* **14,** 891–899
21. Lev, S., Hernandez, J., Martinez, R., Chen, A., Plowman, G., and Schlessinger, J. (1999) Identification of a novel family of targets of PYK2 related to *Drosophila* retinal degeneration B (rdgB) protein. *Mol. Cell. Biol.* **19,** 2278–2288
22. Liou, J., Fivaz, M., Inoue, T., and Meyer, T. (2007) Live-cell imaging reveals sequential oligomerization and local plasma membrane targeting of stromal interaction molecule 1 after Ca^{2+} store depletion. *Proc. Natl. Acad. Sci. U.S.A.* **104,** 9301–9306
23. Hilgemann, D. W., Feng, S., and Nasuhoglu, C. (2001) The complex and intriguing lives of PIP2 with ion channels and transporters. *Science's STKE: Signal Transduction Knowledge Environment* **2001,** re19
24. Nasuhoglu, C., Feng, S., Mao, Y., Shammat, I., Yamamato, M., Earnest, S., Lemmon, M., and Hilgemann, D. W. (2002) Modulation of cardiac PIP2 by cardioactive hormones and other physiologically relevant interventions. *Am. J. Physiol. Cell Physiol.* **283,** C223–C234
25. Levine, T. (2004) Short-range intracellular trafficking of small molecules across endoplasmic reticulum junctions. *Trends Cell Biol.* **14,** 483–490
26. Ile, K. E., Schaaf, G., and Bankaitis, V. A. (2006) Phosphatidylinositol transfer proteins and cellular nanoreactors for lipid signaling. *Nat. Chem. Biol.* **2,** 576–583
27. Cockcroft, S. (2012) The diverse functions of phosphatidylinositol transfer proteins. *Curr. Top. Microbiol. Immunol.* **362,** 185–208
28. Lu, C., Peng, Y. W., Shang, J., Pawlyk, B. S., Yu, F., and Li, T. (2001) The mammalian retinal degeneration B2 gene is not required for photoreceptor function and survival. *Neuroscience* **107,** 35–41
29. Carlisle, F. A., Pearson, S., Steel, K. P., and Lewis, M. A. (2013) Pitpnm1 is expressed in hair cells during development but is not required for hearing. *Neuroscience* **248,** 620–625
30. Brandman, O., Liou, J., Park, W. S., and Meyer, T. (2007) STIM2 is a feedback regulator that stabilizes basal cytosolic and endoplasmic reticulum Ca^{2+} levels. *Cell* **131,** 1327–1339